

A new experimental setup to measure hydraulic conductivity of plant segments

3

4

March 31, 2023

1 Abstract

6 Plant hydraulic conductivity and its decline under water stress is the focal point
7 of current plant hydraulic research. Common methods of measuring hydraulic
8 conductivity control a pressure gradient to push water through plant samples,
9 submitting them to conditions far away from those that are experienced in na-
10 ture where flow is suction driven and determined by the leaf water demand.
11 In this paper, we present two methods for measuring hydraulic conductivity
12 under closer to natural conditions, an artificial plant setup, and a horizontal
13 syringe pump setup. Both approaches use suction to pull water through a
14 plant sample while dynamically monitoring flow rate and pressure gradients.
15 The syringe setup presented here allows for controlling and rapidly changing
16 flow and pressure conditions, enabling experimental assessment of rapid plant
17 hydraulic responses to water stress. The setup also allows quantification of
18 dynamic changes in water storage of plant samples. Our tests demonstrate
19 that the syringe pump setup can reproduce hydraulic conductivity values mea-
20 sured using the current standard method based on pushing water under above-
21 atmospheric pressure. Surprisingly, using both the traditional and our new
22 syringe pump setup, we found a positive correlation between changes in flow
23 rate and hydraulic conductivity. Moreover, when flow or pressure conditions
24 were changed rapidly, we found substantial contributions to flow by dynamic
25 and largely reversible changes in the water storage of plant samples. Although
26 the measurements can be performed under sub-atmospheric pressures, it is not
27 possible to subject the samples to negative pressures due to the presence of gas
28 bubbles near the valves and pressure sensors. Regardless, this setup allows for
29 unprecedented insights into the interplay between pressure, flow rate, hydraulic

30 conductivity, and water storage in plant segments. This work was performed
31 using an Open Science approach with the original data and analysis to be found
32 at <https://doi.org/10.5281/zenodo.7322605>.

33 2 Background and Aims

34 Plant leaves absorb light and CO_2 for photosynthesis, but at the same time
35 they lose water to the atmosphere through transpiration. To replenish water
36 loss, plants entertain an elaborate network of xylem conduits that connect the
37 water uptake tissues in the roots with the evaporating tissues in the leaves.
38 Similarly to porous media, water loss causes tension in the leaves, which drives
39 root-leaf water transport along the pressure gradient between the leaves and
40 the roots, supported by cohesion between water molecules. This is commonly
41 described as the cohesion-tension theory (Dixon and Joly, 1895; Zimmermann
42 et al., 1993; Tyree and Zimmermann, 2002; Shi et al., 2020).

43 Plant water transport through xylem can only be maintained if the pressure
44 drop between roots and leaves is greater than the hydrostatic pressure drop due
45 to the change in gravitational potential between roots and leaves. The drier
46 the soil, the larger the tension in the soil itself, requiring even more tension (or
47 lower water pressure) in the leaves to ensure water transport (Dixon and Joly,
48 1895). These pressures in the xylem are commonly so low that the system is
49 believed to operate in a meta-stable state, where any air seeding in a vessel
50 can cause embolism propagation, resulting in embolisms, which would make a
51 vessel dysfunctional for water transport (Sperry, 1986; Canny, 1998). Here we
52 refer to air seeding as any process that introduces air into the xylem (Tyree and
53 Zimmermann, 2002), such as air entry through pit membranes or wounds.

54 The presence of embolized conduits reduces the efficiency of water trans-
55 port, expressed as a decrease in hydraulic conductivity. The reduced hydraulic
56 conductivity due to embolism has to be compensated for by an increased pres-
57 sure gradient, i.e. lower water pressures in the xylem, in order to maintain
58 an adequate water transport rate. The lower pressure can lead to more em-
59 bolized conduits, resulting in the positive feedback loop of runaway embolism
60 propagation (Tyree and Sperry, 1988; Hölttä et al., 2009).

61 Vulnerability of a plant to embolism spreading and loss of hydraulic conduc-
62 tivity is a primary focus in current plant hydraulic research (McDowell et al.,
63 2019). Many methodological advances have been made to measure the “percent

64 loss of hydraulic conductivity” (PLC) under water stress, but the methods to
 65 measure exact hydraulic conductivity values in plants or plant segments have
 66 received relatively little scrutiny (see, e.g. Cochard et al., 2013; Venturas et al.,
 67 2017). While there is currently a method to measure plant vulnerability in vivo,
 68 micro CT, it does not measure an absolute hydraulic conductivity but a theo-
 69 retical one (Pratt et al., 2020). Therefore, we will not expand on its details in
 70 this paper.

71 In the most common method for measuring plant hydraulic conductivity,
 72 one end of the plant sample is attached to a tube with above-atmospheric liquid
 73 pressure (e.g. a water reservoir that is elevated), while the other is exposed to
 74 atmospheric pressure, where water flows into a reservoir placed on a balance.
 75 The change in weight of the downstream reservoir over time is used to calculate
 76 the flow generated by the hydraulic head. In this paper we will refer to this
 77 method as the “Sperry method” (Sperry et al., 1988; Canny et al., 2007; Torres-
 78 Ruiz et al., 2012). A slight modification to this method was employed by Tyree
 79 and Yang (1992), who added a balance under the supplying reservoir, allowing
 80 to quantify gains in sample water content during refilling of desiccated samples
 81 under pressure. A similar technique to the Sperry method uses a high pressure
 82 flow meter (HPFM), where pressure is generated on one side using compressed
 83 air to push water through a plant sample connected by flexible tubing. The
 84 flow is calculated from the pressure drop across a capillary located between
 85 the plant sample and the pressure generator. In this paper we will refer to
 86 this method as the “HPFM setup” (Tyree et al., 1993). The HPFM setup is
 87 mainly used for measuring the hydraulic conductivity of roots (Tyree et al.,
 88 1995; Tsuda and Tyree, 2000). Yet another modification to the Sperry method
 89 was proposed by Kolb et al. (1996), who measured the hydraulic conductance
 90 of entire branches or root systems by placing them in a vacuum chamber and
 91 connecting the protruding stem with a water reservoir placed on a balance. In
 92 this setup, water is transported through the system by suction and hydraulic
 93 conductance is calculated from the linear relation between flow rate and vacuum
 94 pressure in the chamber. We will refer to this method as the “Kolb setup”.

95 A method that in theory enables conductivity measurements at negative liq-
 96 uid pressure is the Cavitron method (Alder et al., 1997; Cochard et al., 2013),
 97 where a plant sample with rotor cups on each end is placed in a centrifuge, and
 98 the pressure inside the twig is determined by the rotation rate of the centrifuge,
 99 whereas the pressure gradient depends on the position of water menisci in the
 100 rotor cups. The water level of the downstream rotor cup is fixed at the position

101 of its outflow hole, while the water level in the upstream rotor cup is located fur-
 102 ther off-center, thus creating a gradient in water potential between the two ends
 103 of the plant sample. During the experiment, the water level of the upstream
 104 rotor cup slowly recedes as water is transported through the plant sample to-
 105 wards the downstream rotor cup. The flow rate could be calculated by taking
 106 the change in water level in the upstream rotor cup over time and multiplying
 107 it with the cross-sectional area of water in the rotor cup. However, due to the
 108 unknown twig volume in the rotor cup, an exact flow rate, and thus hydraulic
 109 conductivity, is not routinely determined, only the relative loss in conductivity
 110 is recorded as rotation speed is increased.

111 Unfortunately, none of the above methods reproduces the situation *in planta*:

- 112 • In the centrifuge method, the pressure along the twig is non-linear, with
 113 the lowest pressure in the middle (Cochard, 2002), rather than at the sink,
 114 as would be the case in a real plant.
- 115 • In all of the above methods, the pressure difference along the sample
 116 is held constant (atmospheric at the outflow side of the twig and above-
 117 atmospheric at the inflow side for the Sperry and HPFM setups), while the
 118 flow rate adjusts according to the hydraulic conductance of the twig. This
 119 is in contrast to natural conditions in a plant, where the system functions
 120 at sub-atmospheric or even negative liquid pressure and the pressure drop
 121 along the flow path adjusts to the hydraulic conductivity and the flow
 122 rate, the latter of which is determined by the transpiration rate (Venturas
 123 et al., 2017). This means that a sudden decline in hydraulic conductivity
 124 would cause a sudden drop in pressure, which is not the case in the above
 125 methods, which all control the pressure gradient across plant samples such
 126 that in the event of embolism propagation, the flow rate decreases, not
 127 the pressure, as would be expected in an intact plant.
- 128 • Most methods involve above-atmospheric pressures, so water stress cannot
 129 be induced while measuring hydraulic conductivity.

130 Except for the setup by Tyree and Yang (1992), none of the above methods
 131 quantifies changes in water storage of the plant sample, so it is not clear if the
 132 flow measured at one end of the sample constitutes through-flow or if part of the
 133 observed flow is due to emptying or re-filling water storage in the plant sample
 134 (Torres-Ruiz et al., 2012).

135 To fill these methodological gaps, in the present study, we aim to design
136 an experimental setup for measuring hydraulic conductivity closer to natural
137 conditions, with the following goals:

- 138 1. Flow rate controlled, pressure drop as response;
- 139 2. Suction-induced flow;
- 140 3. Ability to simulate water stress in the plant segment;
- 141 4. Ability to measure changes in storage.

142 **3 Materials and Methods**

143 Below, we present two different setups that were designed to achieve the above-
144 mentioned goals. One is an intuitive, low-cost vertical setup resembling an
145 artificial plant. The second is a more controlled horizontal setup, improving on
146 certain shortcomings of the vertical setup.

147 **3.1 Artificial Plant Setup**

148 The initial setup was designed to mimic a plant in the simplest form, containing
149 one evaporating “leaf”, one “root” immersed in a water reservoir, and connect-
150 ing tubes where a plant segment is inserted in a vertical setup (Fig. 1). The root
151 and leaf each is replicated by a Rhizon sampler (Rhizosphere Research Prod-
152 ucts B.V., Wageningen, Netherlands), consisting of a membrane with pores of
153 $5\mu\text{m}$ diameter. Pressure sensors (24PC; Honeywell, Morristown, NJ, USA) are
154 connected through T-valves on either side of the plant segment. A liquid flow-
155 meter (SLG-0150; Sensirion, Stäfa, Switzerland) is inserted in the flow path
156 below the lower pressure sensor. The water reservoir consists of a beaker filled
157 with de-ionized water.

158 Evaporation from the leaf replica generates the suction necessary to pull
159 water up all the way from the beaker, following the cohesion-tension principle.
160 Note that the membranes need to be covered by a continuous water film, oth-
161 erwise air can enter through empty pores and water transpired at the surface is
162 replaced by air, instead of water from below.

163 Initial filling of the system is performed without a twig in place, by placing
164 both membranes in a beaker filled with DI water. A syringe is attached to one
165 of the T-valves, at the position where the twig will be added. The syringe is

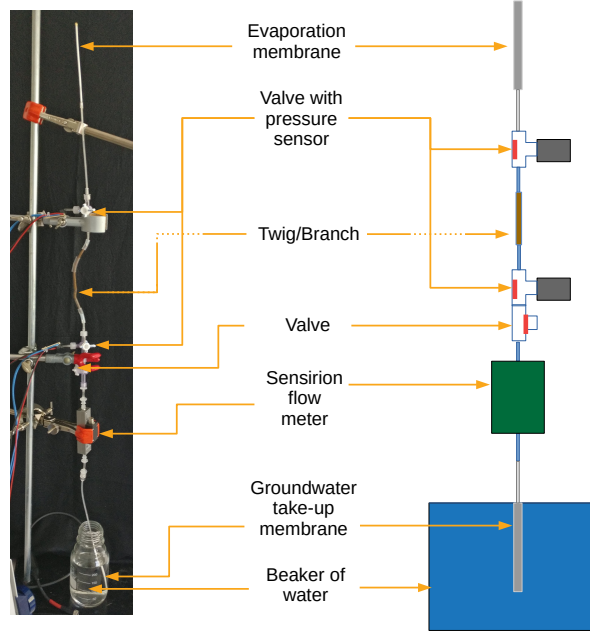


Figure 1: Setup for measuring hydraulic conductivity of twig samples using an evaporation membrane to drive flow.

166 pulled to fill the membrane and tubing with water. Turning the T-valve to only
 167 be open to the syringe and pressure sensor, the sensor is removed and water is
 168 pushed to fill that section and the sensor is re-attached. The process is repeated
 169 with the other side. Finally, the twig sample is attached and the setup is placed
 170 upright with one membrane in the beaker and the other held in the air using a
 171 stand where it begins to evaporate (Fig. 1).

172 3.2 Horizontal Syringe Setup

173 The horizontal syringe setup (Fig. 2) consists of a syringe pump (neMESYS;
 174 Cetoni, Wiesenring, Germany) to control the water flow rate from a beaker
 175 passing through a twig sample. Pressure sensors on either side of the twig and
 176 a flow meter (SLI-0430; Sensirion, Stäfa, Switzerland) in the flow path allow
 177 for the measurement of hydraulic conductivity. Additionally, depending on the
 178 setting of the valves, flow can be passed through a capillary to increase flow
 179 resistance on the upstream side and hence reduce overall pressure in the system
 180 if desired. This setup will be referred to as the “Syringe setup”.

181 The twig-less Syringe setup is filled by pulling water, using the syringe, from
 182 the beaker to the syringe pump through the bypass connecting the pressure
 183 sensors, then detaching the syringe is detached and the air within the syringe
 184 emptied before re-attaching it. The pressure sensors are individually removed
 185 to allow water to be gravitationally pushed to fill up to the connection point,
 186 where the sensors are then re-attached.

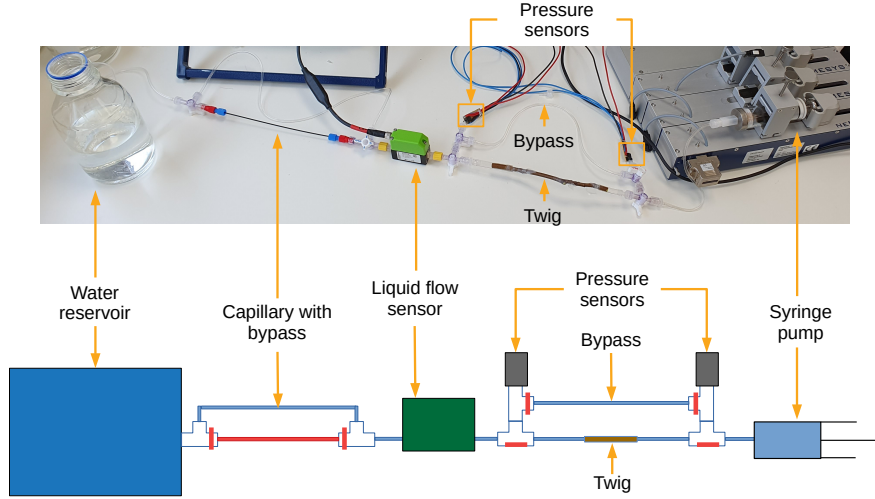


Figure 2: Horizontal syringe setup using syringe pump (g) to control water flow rate to and from the beaker (a). The twig (e) is inserted in the flow path to measure its hydraulic conductivity using flow (c) and pressure (d) meters. The bypass (f) is used to calibrate the sensors before an experiment. A capillary with bypass (b) is used as an example modification to lower the pressure.

187 3.3 Calibration Procedures

188 To avoid spurious results due to sensor drift, the following test and calibration
 189 procedures were followed. The flow sensor is calibrated before each experiment
 190 as there can be instrument drift between experiments due to biological residue
 191 build-up, which can only be eliminated by periodic flushing with alcohol. For the
 192 calibration, water flow is redirected through the bypass around the sample (Fig.
 193 2f) with a direct path between the syringe and water reservoir. Known flow

194 rates are generated using the syringe pump and correlated with measurements
 195 by the flow meter. The calibration is performed using a linear regression and
 196 applied to the data of the following experiment.

197 Pressure sensors were calibrated individually using the relation between pres-
 198 sure and volume obtained from the ideal gas law (Eq. 1).

$$PV = nRT \quad (1)$$

199 In Eq. 1 P is the pressure (Pa), V is the volume of the gas (m^3), n is the
 200 number of moles (mol), R is the gas constant ($\text{K mol Pa}^{-1} \text{ m}^{-3}$), and T is the
 201 temperature (K).

202 Assuming a completely sealed system (n is constant), and a constant tem-
 203 perature during the calibration, a change in the gas volume from V_{ref} to V_{new}
 204 would cause an inversely proportional change in pressure from P_{ref} to P_{new} ,
 205 such that:

$$P_{new} = \frac{P_{ref}V_{ref}}{V_{new}} \quad (2)$$

206 The pressure sensors were attached to the syringe with a small tube and
 207 t-valve which was closed to the atmosphere, the internal volume of which was
 208 considered as the reference gas volume (V_{ref}) and thus needed to be measured.
 209 To do so, we weighed the empty tube and t-valve, before and after filling it with
 210 water. By taking the weight difference between them and dividing it by the
 211 density of water, we obtained the reference gas volume.

212 The pressure sensor measures pressure relative to the atmosphere using two
 213 openings, one open to the atmosphere and one attached to the volume of in-
 214 terest. A membrane between the two openings bends with the difference in
 215 pressures and delivers a voltage based on the amount of inflection. With no
 216 difference (both at atmospheric pressure), no voltage is delivered and 0 V was
 217 measured. After filling the system with air at atmospheric pressure (assumed to
 218 be 101.3 kPa) and recording the measured sensor voltage (0 V), a known change
 219 in volume was applied using the syringe and the corresponding pressure was de-
 220 termined from Eq. 2. This pressure, along with the measured sensor voltage
 221 was recorded. This was repeated in several steps while increasing volume and
 222 decreasing volume again, in order to prevent that any transient in conditions
 223 (e.g. temperature or instrumental drift, or air leaks) would influence the slope
 224 of the calibration. Both sensors were calibrated one after another on the same

day, taking 15 minutes for each sensor. In order to determine if the values of the
 sensors drifted over time, a second calibration was done two years later. The
 data of both calibration sets was pooled together, resulting in a data series of
 22 points for the bottom sensor, with pressures ranging between 2.56 kPa and
 101.3 kPa, and 21 points for the top sensor, with pressures ranging between 2.68
 kPa and 101.3 kPa. Linear least square fits through the data gave Pearson's
 correlation coefficients of $r > 0.998$ for each sensor. Due to the high correla-
 tion coefficients for the pooled data, suggesting minimal instrument drift, the
 slope and intercept of the pooled calibration data were applied to all experimen-
 tal data presented here. Furthermore, any biases that would remain from this
 method cancel out when calculating the pressure difference between the sensors
 (ΔP) for measuring conductivity. To further counteract potential instrumental
 drift, before each experiment, the difference in pressure between the two sensors
 is measured at two points to remove any offsets. The first point is measured
 before an experiment when the sensors are at atmospheric pressure. The second
 point is the lowest attainable liquid pressure reachable with the setup, i.e. the
 water vapor pressure, which is measured once the experiment has concluded.
 The latter is measured by closing valves such that the syringe is only connected
 to both sensors via the bypass and flow cannot occur. The syringe is set to
 pull at $250 \mu\text{L min}^{-1}$, and as in-flow is stopped, pressure lowers to the vapor
 pressure where gas bubbles form and the pressure no longer decreases. The
 flow is continued for 20 minutes. The water vapor pressure measurement occurs
 after the experiment as the measuring process fills the setup with gas. From the
 two points, a linear regression of the difference between the pressure sensors is
 calculated and a correction is applied to remove potential offsets.

3.4 Sample Collection and Connection

All twig samples used in this paper were collected from *Fagus sylvatica* in Bel-
 val, Luxembourg, following Wheeler et al. (2013) to avoid having any artificial
 embolism propagation in the sample. The branch is cut from the tree and left
 to sit in a bag for at least 30 minutes. The branch is then re-cut under water,
 cutting at least one mean vessel length from either side of the sample to make
 sure that any embolism due to the initial cut is removed. For samples in this
 paper, 10 cm are removed from each end, as Buchmüller (1986) found that 40%
 of the dry wood samples of *Fagus sylvatica* had a maximum vessel length of un-
 der 8 cm, with an additional 30% of samples having a maximum vessel length

between 8 and 16 cm. Any branches along the cut segment are removed under water and sealed with parafilm and/or silicon gel to avoid air entry. Flexible tubing is attached to both ends of the submerged twig, then removed from the water and connected to either side of the setup. The diameter of the samples varied between 3.8 and 4.2 mm. We did not measure the diameter for all the samples, thus a value of 4.0 mm was used for the calculations (see below).

3.5 Conductivity Calculation

Flow through a porous medium such as the twig xylem can be described using Darcy's Law (Eq. 3):

$$Q_m = \frac{kA\rho}{\mu L} \Delta P \quad (3)$$

where Q_m is the mass flow rate (kg s^{-1}), k is the intrinsic permeability (m^2), A is the cross sectional area of the whole twig (m^2), ΔP is the pressure drop along the flow path (MPa), μ is the dynamic viscosity ($\text{MPa} \cdot \text{s}$), and L is the length of the segment (m). The mass flow rate can be converted to a volumetric flow rate (Q_v , $\text{m}^3 \text{s}^{-1}$) by multiplying the mass flow rate by the density of water:

$$Q_v = \frac{Q_m}{\rho} \quad (4)$$

In the literature, the efficiency of water transport through a twig sample is expressed in different ways, which have different relations to intrinsic permeability (k) and are expressed in different units. For example, some authors use specific conductivity, which is affected by viscosity, $K_S = \frac{k\rho}{\mu}$ ($\text{kg m}^{-1} \text{MPa}^{-1} \text{s}^{-1}$), others use specific conductance, which is affected by viscosity and sample length, $K_{AS} = \frac{k\rho}{\mu L}$ ($\text{kg m}^{-2} \text{MPa}^{-1} \text{s}^{-1}$) (Caquet et al., 2009). In some cases, e.g. Bär et al. (2018); Rosner et al. (2019), the units of specific conductivity were reported as ' $\text{m}^2 \text{MPa}^{-1} \text{s}^{-1}$ ', which are obtained by substituting the volumetric flow rate (Eq. 4) for the mass flow rate in Eq. 3.

Note that viscosity is temperature dependent and therefore specific hydraulic conductivity values should only be compared between measurements performed at similar temperatures. All the experiments presented in this paper were conducted in an air conditioned lab around 21 °C and humidity between 25 and 40%. Continuous temperature measurements in a 500 ml beaker of water in the same lab revealed that the water temperature varied between 21 and 23 °C over

the duration of 2 weeks in September 2022, with a maximum temporal variation by 0.6 K in 2 hours. Whenever temperature was needed for calculations, we used a temperature of 21 °C.

For easier comparison with literature values, we do not report intrinsic permeability, but calculated the specific hydraulic conductivity of twig samples using the formulation of Sperry et al. (1988):

$$K = \frac{Q_V \rho L}{\Delta P A} \quad (5)$$

where K is the hydraulic conductivity ($\text{kg m}^{-1} \text{MPa}^{-1} \text{s}^{-1}$), ρ is the density of water (kg m^{-3}). The pressure drop (ΔP) was measured by pressure sensors on both sides of the twig, as described above. The length of the twig is measured as the distance between the centers of the cuts on each side. The cross-sectional area (A) is calculated from the stem diameter assuming a circular shape. The flow rate in the syringe setup is measured by the syringe pump (as a set flow rate out of the twig), and the flow sensor (as an instantaneous flow rate into the twig). Unless otherwise noted, the flow meter measurements were used to calculate conductivity in this paper as these resulted in more stable conductivity values (see also SI Fig. S3).

3.6 Experiments

In the first experiment, the artificial plant setup was left to evaporate to test the measurement of flow, pressure difference, and conductivity change over time. Then, we attempted to produce runaway embolism propagation by adding a gas bubble to initiate embolism. The gas bubble was the width of the tubing and 1.5 times the width in length, and was added through a valve below the lower pressure sensor and rose to the twig while flow, pressure, and hydraulic conductivity were being measured.

The remaining experiments were conducted using the horizontal syringe pump setup. First, the setup was compared with the current standard, the Sperry method, to verify if similar values of hydraulic conductivity are obtained using either method. For direct comparison, both methods were applied consecutively using the same sample. The Sperry method was applied by disconnecting the syringe pump (g in Fig. 2), and letting the water drain freely while elevating the beaker at the other end of the setup (a in Fig. 2) to create the desired pressure difference. The beaker was elevated to 35.5 cm for 30 minutes, then to

321 73.5 cm for 30 minutes, then to 104.9 cm for 30 minutes, and then returned to
322 73.5 cm for another 30 minutes, before returning to 35.5 cm for 30 minutes.

323 After this set of measurements, the beaker was placed back on the table, and
324 the syringe pump was re-attached. Water was pulled through the sample (in the
325 same flow direction as before) at flow a rate of $10 \mu\text{L min}^{-1}$ for 30 minutes, then
326 at $20 \mu\text{L min}^{-1}$ for 30 minutes, then at $30 \mu\text{L min}^{-1}$ for 30 minutes, then again
327 at $20 \mu\text{L min}^{-1}$ for 30 minutes, before returning to $10 \mu\text{L min}^{-1}$ for another 30
328 minutes.

329 The next experiment was designed to simulate water stress in plants using
330 the syringe setup. Two types of water stress were simulated, (a) reduced water
331 supply (e.g. due to soil moisture drought), and (b) increased leaf water demand
332 (e.g. in the mornings, or due to wind gusts or sunflecks). To simulate soil mois-
333 ture drought, water flow between the beaker and the twig was deviated through
334 a capillary by turning the valves in Part b of Fig. 2, resulting in increased flow
335 resistance upstream of the twig and hence reduced pressure. Increased water
336 demand was simulated by increasing the flow rate induced by the syringe pump,
337 increasing the pressure gradient along the twig.

338 The final experiment was designed to quantify the change in twig water
339 storage between a relaxed condition (zero flow, e.g. at night) and flow under
340 tension (e.g. during the day). In this experiment, the syringe setup was started
341 in the same way as in the soil moisture drought experiment, i.e. water was
342 passed through a capillary before reaching the twig. When the measured flow
343 rate into the twig became roughly steady, the syringe pump was stopped and
344 the subsequent slow decay in flow rate was monitored until flow was no longer
345 detected. Differences between syringe pump flow and the flow meter signal were
346 interpreted as rate of change in twig storage.

347 4 Results

348 4.1 Conductivity Measurement with Artificial Plant Setup

349 Time in the graphs begins at 0 with the start of the experiment, which repre-
350 sents the first time flow was induced. This was either when the membrane was
351 removed from water, the beaker was moved to a higher elevation, or the flow
352 was started with the syringe pump.

353 A 2.2 cm long twig was attached to the artificial plant setup and left to
354 evaporate. The flow rate started at $2.5 \mu\text{L min}^{-1}$ and increased steadily to

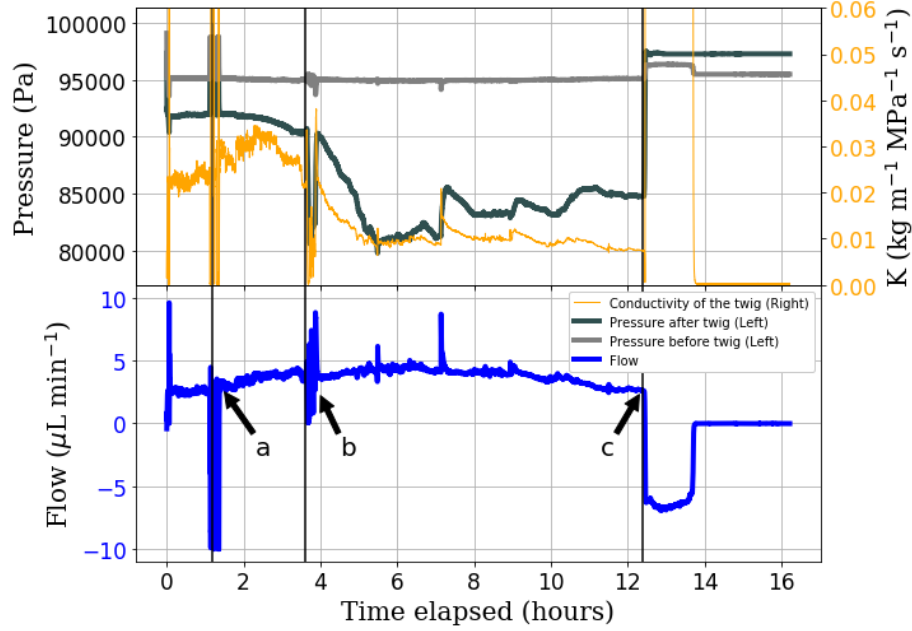


Figure 3: Flow, pressure, and conductivity measurements of a 2.2 cm *Fagus sylvatica* sample in the artificial plant setup. Air bubble was added below the lower pressure sensor 'a', and reached the sample at time 'b'. Air entered the membrane at the top and flow reversed at 'c'.

355 4.0 $\mu\text{L min}^{-1}$ over the first 3.7 hours of the experiment. During this time, the
 356 pressure above the twig slowly decreased from 93 kPa to 91.5 kPa (Fig. 3).
 357 The conductivity of the sample increased from 0.023 to 0.025 $\text{kg m}^{-1} \text{MPa}^{-1} \text{s}^{-1}$
 358 s^{-1} over the first hour. The air bubble was added at 1.5 hours (Fig. 3a) while
 359 conductivity continued to increase to a peak of 0.033 $\text{kg m}^{-1} \text{MPa}^{-1} \text{s}^{-1}$ at
 360 the 2.3 hour point and then decreased again to 0.027 $\text{kg m}^{-1} \text{MPa}^{-1} \text{s}^{-1}$ at
 361 3.7 hours, when the bubble reached the sample. At this point, flow dropped
 362 to 0 and pressure decreased rapidly to 80.7 kPa (Fig. 3b), at which point the
 363 air bubble began passing through the twig. After 15 minutes we were able to
 364 observe air bubbles coming out of the twig on the upper side, indicating that
 365 at least part of the gas in the introduced bubble passed through the whole twig
 366 and left it again at the other end. The pressure returned to the previous 91.5
 367 kPa, and flow resumed at 4 $\mu\text{L min}^{-1}$. The flow remained relatively stable for
 368 the next 1.5 hours while both pressure and conductivity decreased markedly
 369 (from 91.5 kPa to 80.7 kPa and from 0.021 to $1.0 \times 10^{-8} \text{ kg m}^{-1} \text{MPa}^{-1} \text{s}^{-1}$,

370 respectively) during this time. Both pressure and conductivity stayed relatively
 371 steady for the next 6 hours until air entered the upper membrane from outside at
 372 12.5 hours (Fig. 3c). The upper pressure increased and flow reversed, draining
 373 water from the setup above the twig, until the water meniscus stopped at the
 374 top of the twig.

375 4.2 Horizontal Syringe Setup vs. Sperry Method

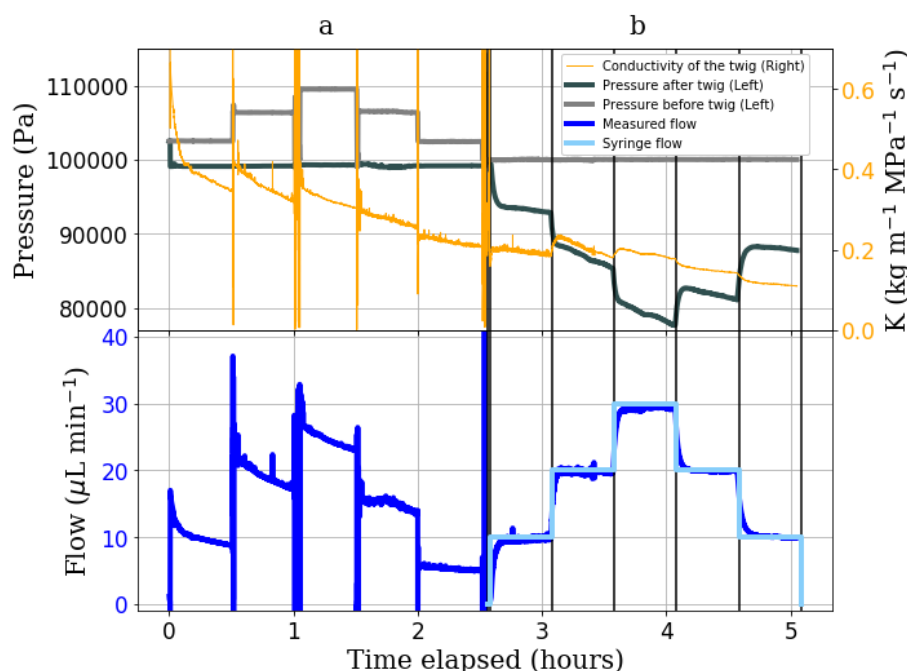


Figure 4: Pressure, flow, and conductivity measurements of a 10.2 cm twig sample over time. Section 'a' represents measurements when water is pushed through a twig sample using controlled pressure differences (Sperry method). Section 'b' represent measurements when water is pulled through the same sample in the same direction using a syringe pump (Syringe setup).

376 During the Sperry method (Fig. 4a), conductivity decreased steadily by 66%
 377 over the total 2.5 hours. When the pressure gradient was increased at 0.5 hours,
 378 there was a step increase in conductivity from 0.36 to 0.41 $\text{kg m}^{-1} \text{MPa}^{-1} \text{s}^{-1}$.
 379 Similar increases in conductivity were observed every time the pressure gradient
 380 was increased, but only one of two step decreases in pressure gradient resulted
 381 in an evident decline in conductivity (at 2 hrs, not at 1.5 hrs). Also when the

method switched from Sperry method to Syringe at 2.5 hours, the hydraulic conductivity was not affected and remained at $0.21 \text{ kg m}^{-1} \text{ MPa}^{-1} \text{ s}^{-1}$ during the transition. Over the 2.5 hours of the syringe pull (Fig. 4b), conductivity also decreased (decreased 50% over 2.5 hours), but more slowly than during the Sperry method. Whenever flow rate was increased, there was a step-wise increase in conductivity, and whenever flow rate was decreased, there was a slight step-wise decrease in conductivity.

When the different hydraulic heads were applied in the Sperry method (Fig. 4a), the pressure was constant and the flow rate decreased over time. However, when different flow rates were applied in the Syringe method (Fig. 4b), it was the pressure that decreased over time while flow was constant.

4.3 Simulating Water Stress

In Fig. 5, the letters ‘a’ through ‘g’ indicate a change to the experimental setting. In Segment ‘a-b’, a constant pull was applied through the twig at $25 \mu\text{L min}^{-1}$ with no flow through the capillary, representing a steady evaporation of the leaf during the day at unrestricted water supply. This reference scenario was established in Segments ‘a-b’, ‘d-e’, and ‘f-g’, for direct comparison to the stress conditions.

Drought stress is simulated at ‘b’, where flow was redirected through a capillary upstream of the twig. In Segment ‘b-c’, flow initially stopped and pressure before the twig decreased sharply, followed by a decrease in pressure after the twig, and slow recovery of flow and conductivity, which reached $0.23 \text{ kg m}^{-1} \text{ MPa}^{-1} \text{ s}^{-1}$ before declining again. When the syringe pump was stopped at ‘c’, flow decreased from 19 to $3 \mu\text{L min}^{-1}$ over the course of an hour, in Segment ‘c-d’, while pressures increased. Conductivity remained similar to that in Segment ‘a-b’, around $0.20 \text{ kg m}^{-1} \text{ MPa}^{-1} \text{ s}^{-1}$.

At ‘d’, the syringe pump was turned on again and the capillary bypassed, as in Segment ‘a-b’. When the pump was turned on, flow rate increased instantly, accompanied by a step increase in conductivity from 0.15 to $0.26 \text{ kg m}^{-1} \text{ MPa}^{-1} \text{ s}^{-1}$. Note that the measured flow rate was initially even higher than the syringe pump flow rate in Segment ‘d’.

Increase in water demand was simulated at ‘e’, where water flow through the twig was increased from 25 to $50 \mu\text{L min}^{-1}$. The flow change was immediately reflected by the flow meter and pressure after the twig decreased suddenly from 85 kPa to 74 kPa , while the conductivity increased from 0.30 to 0.35 kg m^{-1}

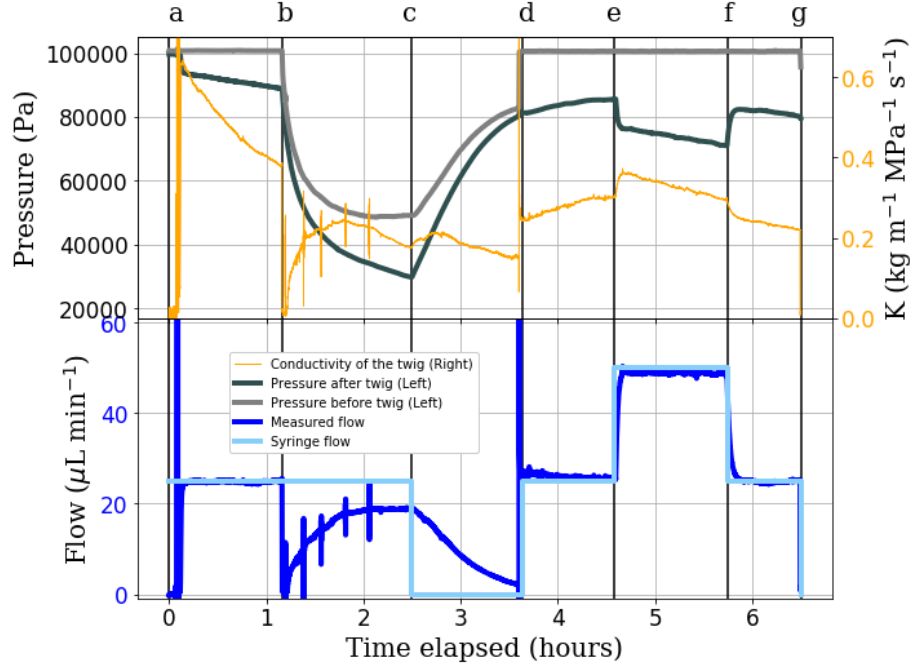


Figure 5: Time series of pressure, flow, and conductivity of a 13.5 cm twig when simulating different sorts of water stress. At ‘a’, a constant pull through the twig at $25 \mu\text{L min}^{-1}$ is applied and flow goes around the capillary. At ‘b’, flow is lead through a capillary upstream of the twig. At ‘c’, the syringe pump is stopped. At ‘d’, conditions are similar to ‘a’. At ‘e’, flow is further increased to $50 \mu\text{L min}^{-1}$. At ‘f’, the system returned to the same conditions as ‘a’ and ‘d’. The experiment ends at ‘g’.

417 $\text{MPa}^{-1} \text{s}^{-1}$, followed by a steady decline in Segment ‘e-f’ from 0.35 to 0.30 $\text{kg m}^{-1} \text{MPa}^{-1} \text{s}^{-1}$.
 418 $\text{m}^{-1} \text{MPa}^{-1} \text{s}^{-1}$.

419 Once the original flow of $25 \mu\text{L min}^{-1}$ was re-established at ‘f’, pressure after
 420 the twig increased again to almost its original value at ‘e’, whereas conductivity
 421 showed another step decrease from 0.29 to $0.26 \text{ kg m}^{-1} \text{MPa}^{-1} \text{s}^{-1}$. Conductivity
 422 in Segment ‘f-g’ decreased steadily from 0.26 to $0.22 \text{ kg m}^{-1} \text{MPa}^{-1} \text{s}^{-1}$.
 423 The overall decrease in conductivity throughout the experiment could be seen
 424 in Fig. 4-6.

4.4 Twig water storage

To better understand if the deviations between syringe pump and flow meter flow rates observed in the previous experiment were related to changes in twig water storage, Segments ‘a-d’ were repeated with a new twig, but with a longer period without syringe pump flow at the end. Changes in storage were calculated as the cumulative difference between the flow rates at the syringe pump and the flow meter.

At the start of the storage experiment (Fig. 6 Segment ‘a-b’), the same pattern of declining conductivity as in the stress experiment was found. When the flow was passed through the capillary at ‘b’, the measured flow rate briefly declined to 0, followed by a steady recovery, reaching a steady rate of $21.7 \mu\text{L min}^{-1}$ at ‘d’, $3.3 \mu\text{L min}^{-1}$ lower than the syringe flow. Interpreting the difference in flow rates as a change in twig water storage, this would suggest that the amount of water in the twig decreased by $475 \mu\text{L}$ at ‘d’. When the syringe pump was turned off (Segment ‘d-e’) the flow meter kept recording flow into the twig, suggesting re-filling of the twig water storage until the flow ceased entirely after another 1.5 hours. At this point, our calculation would suggest a remaining twig water deficit of $175 \mu\text{L}$ (light blue line in bottom panel of Fig. 6).

The difference between the steady state flow rate measured by the flow meter at ‘d’, and the flow rate imposed by the syringe pump suggests that a leak occurred in the system, as a steady-state difference cannot be explained by changing storage. In addition, we observed a bubble in the syringe, confirming the presence of an air leak. The leak was assumed to have formed at ‘c’ due to a slight kink in the pressure, which would likely occur when air entry is initiated. In the absence of more detailed information, the air entry rate was assumed constant in Segment ‘c-d’ and to be equal to the flow rate difference between the steady state flow at ‘d’ and the syringe flow. Using the flow rate based on the assumed air entry rate, storage would have decreased by a maximum of $300 \mu\text{L}$ at ‘d’ and the end storage at ‘e’ would have been $7 \mu\text{L}$ larger than the initial twig water storage at ‘a’.

5 Discussion

In this paper we presented two different methods for measuring hydraulic conductivity under suction and flow-controlled conditions. The first method is an

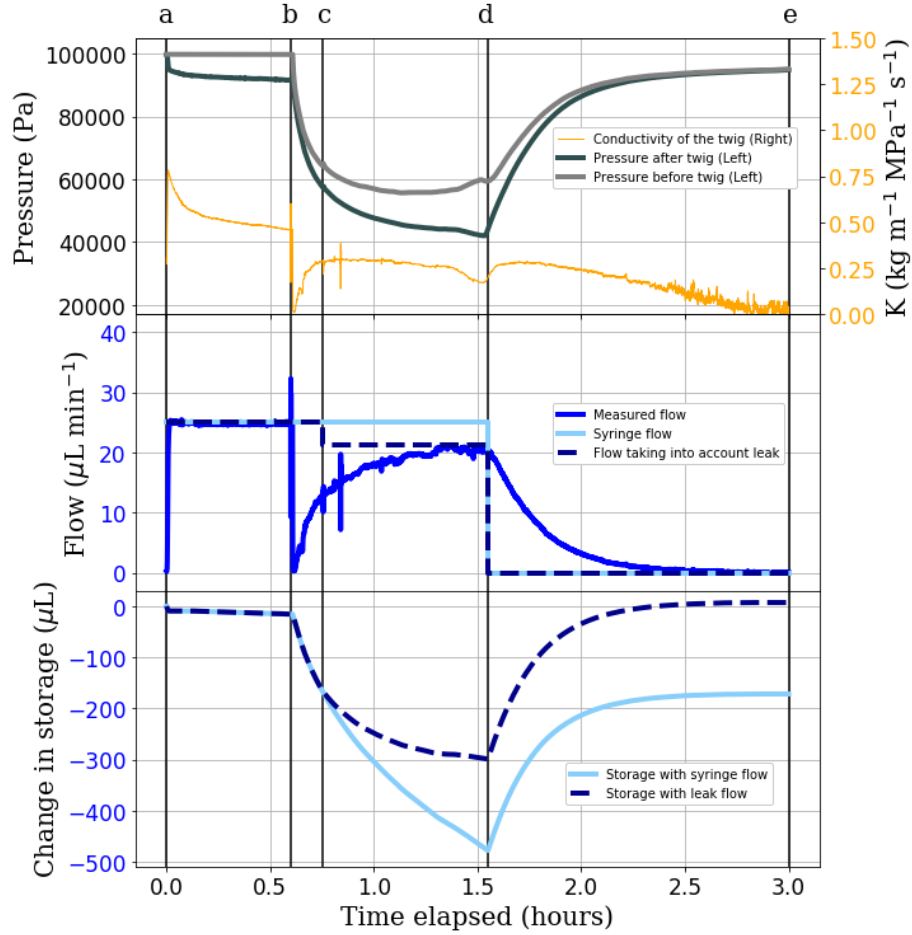


Figure 6: Graph of pressure, flow, conductivity, and storage changes when simulating water stress on a 11.4 cm twig. At ‘a’, a constant pull through the twig at $25 \mu\text{L min}^{-1}$ was applied and flow went around the capillary. At ‘b’, flow was lead through the capillary. At ‘d’, flow was stopped. The experiment ended at ‘e’. Change in storage was calculated as the cumulative difference between measured flow and syringe flow. An air leak was assumed to have formed at ‘c’, see main text.

459 intuitive representation of an artificial plant as an evaporating leaf, transport
 460 tissues, and a root, but it does not offer precise control of the flow. In numerous
 461 experiments using this method (not all shown here), we found that stable flow
 462 could be maintained for many hours, but invariably, sudden, catastrophic fail-
 463 ure occurred by air entry through the evaporating microporous membrane after

464 many hours. An interesting feature of this setup is its educational value, as its
465 vertical orientation and components are intuitively associated with key macro-
466 scopic components of the plant hydraulic system. In this evaporation-driven
467 experimental setup, flow rate continued even when the flow was temporarily
468 constricted, providing the inspiration for a fully flow controlled horizontal setup
469 using a syringe pump to control the flow (second method).

470 This second method is of more scientific value, as it allows for more precise
471 control of flow rate and quantification of twig storage changes as flow rates are
472 known for both sides of the twig. Estimations of twig water storage changes
473 can also be enabled by adding a second balance in the Sperry setup (Tyree
474 and Yang, 1992), but here we avoid evaporation from the beakers, which could
475 cause artifacts in the flow measurements. Our method combines the advantage
476 of quantifying changes in twig water storage with the advantage of measuring
477 conductivity by suction instead of above-atmospheric pressure, as proposed by
478 Kolb et al. (1996), who pointed out that the large pressures needed to measure
479 samples with low conductance (e.g. due to partial embolism) would lead to re-
480 filling of embolised vessels and therefore over-estimate conductance. Therefore,
481 measurements under suction are expected to lead to more accurate hydraulic
482 conductivity values. Since the pressure is measured on both sides of the twig
483 in our setup, we can add an additional resistance (such as a capillary) to the
484 upstream side of the twig to reduce the pressure in the twig. Note that although
485 a sub-atmospheric pressure could also be achieved by elevating the twig relative
486 to the water reservoirs in the setup by Tyree and Yang (1992), for the pressure
487 drop of 70 KPa shown in Fig. 5, the twig would have to be elevated to a height
488 of 7 m, so that setup can only be used for very mild reductions in pressure. In
489 essence, our second method combines the advantages of both setups presented
490 by Tyree and Yang (1992) and Kolb et al. (1996), with the additional bonus
491 of controlling flow while the pressures adjust, which is more representative of a
492 situation where flow is driven by evaporation.

493 The two setups presented here are able to provide different scientific in-
494 sights and highlight different challenges for the quantitative understanding of
495 flow through plant segments. In the artificial plant setup, where we introduced
496 an air bubble below the twig, we were able to see a sudden decline in liquid
497 pressure on the leaf side as the bubble reached the twig, but then, surprisingly,
498 as the pressure difference reached a threshold of 15 kPa (Fig. 3b), the bubble
499 started entering the twig and pressure returned to its original value within tens
500 of minutes. Contrary to expectations that air entry would lead to reduced or

discontinued flow through the hydraulic system, flow and evaporation continued
 at the original rate throughout this experiment, with only short-term pertur-
 bations when the bubble was introduced and when it passed through the twig.
 This was despite a marked decrease in hydraulic conductivity from 0.035 to
 0.010 kg m⁻¹ MPa⁻¹ s⁻¹ during the experiment. It is not clear if the decline in
 hydraulic conductivity was caused by the added air or independent of it, as the
 decreasing trend was observed before the bubble reached the twig, and the same
 trend continued after it had passed through the twig. Note that the behavior
 documented here was only observed with a twig that was shorter than its aver-
 age xylem vessel length (here a twig of 2.2 cm was used, cf. an average xylem
 vessel length of under 8 cm for *Fagus sylvatica* (Buchmüller, 1986)). When a
 longer twig of 12.3 cm was used (SI, Fig. S2), flow declined to zero shortly
 after the bubble reached the lower twig end after 4.2 hours. In this case, the
 bubble did not pass through the twig, blocking flow completely and eventually
 leading to air entry through the evaporating membrane and failure after 5.9
 hours (SI, Fig. S2). This illustrates that there was no vessel longer than 12.3
 cm present in the sample, and that air could not pass from one vessel to an-
 other, such that flow was completely blocked. In the artificial plant setup, any
 gas bubbles transported with the water accumulated at the top of the artificial
 leaf, presumably allowing water supply to the evaporating sites only through a
 thin film along the membrane. This increased resistance to flow likely created
 a large pressure drop between the bulk water and the evaporating sites at the
 tip, eventually resulting in air entry at the top of the membrane. When the air
 entry value of the evaporating membranes was tested without a twig and air
 bubbles, we found sudden air entry at liquid pressures between 35 and 57 kPa,
 which is consistent with the reported pore sizes of the membrane (see SI, Fig.
 S1). The accumulation of air bubbles at the evaporating sites and subsequent
 hydraulic failure highlights the importance of mechanisms to not let air bub-
 bles accumulate in the hydraulic system, even in the absence of negative liquid
 pressures.

To avoid hydraulic failure of the system due to accumulation of air in the
 evaporation membrane and fluctuations in flow rate due to variations in lab
 humidity or air movement around the evaporating membrane, we developed
 the horizontal syringe setup, which also improves on the previous design by ar-
 ranging the setup horizontally, and hence avoiding the offset between pressure
 sensors due to gravitational potential and ensuring that the pressure difference
 measured by the sensors does actually represent the pressure drop along the

538 twig. Note that branches can grow horizontally, so a horizontal setup is not less
 539 “natural” than a vertical one. The replacement of the evaporation membrane
 540 by a syringe pump eliminates the pressure limitation due to the membrane’s air
 541 entry pressure, and fluctuations in flow caused by fluctuations in evaporation
 542 from the membrane. For the same reason, the use of a rhizon on the water
 543 uptake side was also abandoned. The original idea was to place the rhizon in a
 544 porous material to simulate the reduced liquid pressure exerted by the soil, but
 545 with the rhizons used, the pressure could not be lowered below the air entry
 546 pressure of the membrane. Instead, a capillary was used to reduce pressure on
 547 the receiving side of the twig. The syringe pump allows the flow rate to be
 548 precisely controlled through either suction or pushing, as opposed to the evapo-
 549 ration from the membrane. The horizontal syringe setup and the Sperry method
 550 gave comparable values for hydraulic conductivity of the same sample (Fig. 4).
 551 Furthermore, the overall trend in the conductivity over time is maintained when
 552 swapping between the two methods. The step increase and decrease patterns,
 553 when changing pressure difference or flow rate, were seen in both methods, sug-
 554 gesting that the results are likely not of methodological nature, but biological.
 555 The specific hydraulic conductivity was measured between 0.20 and 0.60 kg
 556 m⁻¹ MPa⁻¹ s⁻¹, 3 to 4.5 times lower than literature values: 2.5 kg m⁻¹ MPa⁻¹
 557 s⁻¹ in Rosner et al. (2019) using the Sperry method, and 1.83 kg m⁻¹ MPa⁻¹
 558 s⁻¹ in the Xylem functional traits database (<https://xylemfunctionaltraits.org/>)
 559 Choat et al. (2012). As pointed out by Kolb et al. (1996), the higher conductiv-
 560 ity values reported in the literature could be due to the filling of empty vessels
 561 when samples were flushed with water at high pressures.

562 In all our experiments, we observed continuous declines in hydraulic conduc-
 563 tivity during measurements, which have also been reported before and largely
 564 attributed to microbial growth (Sperry et al., 1988). To avoid the decline in hy-
 565 draulic conductivity and to mimic xylem sap, it has been suggested to add HCl,
 566 KCl, or oxalic acid to the perfusing solution (Sperry et al., 1988; Kolb et al.,
 567 1996; Nardini et al., 2011). However, a decline in K under large pressure gra-
 568 dients even with de-gassed KCl solution and bactericide was found in a study
 569 by Bonetti et al. (2021). This decline could easily be investigated further using
 570 the syringe setup, especially the question whether the decay is due to pressure
 571 or flow rate, which cannot be done with any of the current setups.

572 Here we also note that the previously reported declines were over timescales
 573 of tens of hours (Sperry et al., 1988), whereas our experiments only lasted a
 574 few hours. Therefore we used de-ionized water and were surprised to see the

largest declines within the first half-hour in our horizontal experiments (Figs. 4 - 6). Note that in our vertical experiments, where the flow rate was much lower, the initial decline in conductivity was not observed (Fig. 3 and Fig. S1). This could imply that the decline in hydraulic conductivity was not so much due to microbial growth as to the accumulation of bubbles at the pit membranes (Canny et al., 2007). More experiments using different flow rates would be needed to separate these processes more clearly.

The comparable hydraulic conductivity measurements between the Sperry method and the horizontal syringe setup, along with approximately similar results to literature values confirm that the horizontal Syringe method is a valid alternative to the Sperry method for measuring hydraulic conductivity. In addition, the syringe setup was able to measure hydraulic conductivity while simulating water stress conditions. Simulated soil moisture stress caused a decrease in the pressure on both sides of the twig sample (Fig. 5), which is not possible using the Sperry or HPFM methods, as they rely on fixed pressure gradients and above-atmospheric pressure. Surprisingly, our experiment showed that an increase in flow rate increased the conductivity of the sample, both at constant pressure difference (Sperry method) and constant flow rate (Syringe method). Conversely, step decreases in flow rate resulted in step reductions in conductivity in three out of four cases in Fig. 4. Since flow rates are positively correlated with pressure in the Sperry method (increase in pressure drives flow), but negatively correlated with pressure in the Syringe method (increase in suction drives flow), the combination of both methods allows the conclusion that the sample's conductivity indeed depends on the flow rate, not the liquid pressure. The positive correlation between flow rate and hydraulic conductivity was also found in Fig. 5, at the transitions marked as d, e, and f. More targeted experiments on different species could shed light into potential mechanistic reasons for this behaviour.

Another advantage of the syringe pump setup is that the flow rate is measured on both sides of the twig, giving additional information about the state of experiments. When pulling water through a sample, the water leaving the twig is determined by the syringe pump, while the flow entering the twig is measured by the liquid flow meter at the other end. In our experiments, it has enabled the detection of leaks or changes in the twig's storage (Fig. 6). The following processes can cause a deviation between the measured flow (Q_m) and the syringe pump flow rate (Q_s):

- 611 1. Changes in water storage of the system between the flow meter and the
612 syringe pump. This could result in $Q_m > Q_s$ or $Q_m < Q_s$.
- 613 2. Evaporation of water from the twig. This would result in $Q_m > Q_s$.
- 614 3. Air seeding or exsolution of gas between the flow meter and the syringe
615 pump. This would result in $Q_m < Q_s$. Air bubbles should become visible
616 in the tubes or the syringe pump in this case.

617 To quantify the storage changes in the tubing, we ran an experiment similar
618 to Fig. 6, but without a twig. The results suggested that a significant deviation
619 in flow rates between the syringe pump and flow meter could only be maintained
620 for a few minutes and the total change in storage was less than 60 μL (SI Fig.
621 S4). Since we never observed persistently greater flow meter values compared
622 to the syringe pump, we can exclude a significant contribution of evaporation
623 from the twig. The only occurrences of $Q_m > Q_s$ were found for a limited
624 time after reductions in flow rate, implicating changes in storage as the reason.
625 In two cases, we documented persistently $Q_m < Q_s$, both under conditions
626 of low pressure, and associated with the accumulation of gas in the syringe,
627 indicating that air might have entered. In general, if Q_m deviates from Q_s but
628 then converges, this indicates that the system storage is adjusting to a new
629 steady state. In Figs. 5 and 6, we found clear indications of changes in storage,
630 some of which were followed by indications of temporary leaks or gas exsolution
631 periods (persistently $Q_m < Q_s$ in Fig. 5b-c, and Fig. 6c-d). In Fig. 6, we
632 calculated the change in storage from the cumulative sum of $Q_s - Q_m$ and used
633 the steady value of $Q_s - Q_m$ in Fig. 6c to quantify the hypothesized air entry
634 rate. Remarkably, when accounting for this air entry, assumed to occur only
635 at a liquid pressure below 55 kPa (based on a slight bump in the pressure and
636 flow data at this threshold), the storage deficit gradually returned to zero 1.5
637 hours after switching the syringe pump off. This indicates the capacity of the
638 twig to reversibly reduce and replenish its storage depending on the flow rate
639 and pressure applied.

640 This elastic storage component may also be the reason for the so-called
641 ‘passive water uptake’ commonly found when using the Sperry method, which
642 is then subtracted from the measured flow rates to achieve more consistent
643 results (Torres-Ruiz et al., 2012). Since the magnitude of the ‘passive water
644 uptake’ increases with the xylem tension prior to the experiment (Table 1 in
645 Torres-Ruiz et al., 2012), it is likely that the underlying mechanism is the same

646 as that causing water flow into the twig in our experiments at zero syringe
 647 pump flow rate after the water stress treatments (Figs. 5 and 6). The dynamic
 648 decay of this spontaneous water uptake observed in our experiments is consistent
 649 with the interpretation that it is likely related to a relaxation of elastic tissues
 650 (Zweifel et al., 2001). However, since the dynamics of flow during a conductivity
 651 measurement is usually not reported, we cannot tell in how far the ‘passive
 652 water uptake’ analysed by Torres-Ruiz et al. (2012) is indeed related to the
 653 elastic relaxation seen in our experiments, and if it was, how a constant rate
 654 of ‘passive water uptake’ could be deduced from such a dynamically decaying
 655 curve. Fortunately, the ability to measure flow rate on both sides of the twig in
 656 our setup gives us a clear indication of any artifacts in the flow measurements,
 657 and to our surprise, conductivity calculations based on the measured flow rate of
 658 water into the twig and the pressure gradient along the twig produced consistent
 659 conductivity values even during moderate emptying or re-filling of the twig water
 660 reservoir (see e.g. conductivity values before and after Point d in Fig. 6). Note
 661 that the change in storage of our system without a twig is an order of magnitude
 662 smaller than the change in storage observed in the presence of a twig (SI Fig.
 663 S4 and S5), so we can rule out an artifact due to elasticity in our system.

664 The experiments presented here were not designed to gain any particular
 665 scientific insights, but to illustrate the capabilities and potential limitations of
 666 the newly presented methods. The main limitation of both methods is that the
 667 liquid pressure cannot be lowered sufficiently to induce significant loss of con-
 668 ductivity during a flow measurement. Even if the valve upstream of the twig is
 669 closed while the syringe pump is sucking, liquid pressure only decreases down to
 670 the saturation vapour pressure of the water in the tubes, i.e. around 3 kPa at 25
 671 °C, at which point cavitation occurs, triggered by any gas bubble in the system,
 672 including those inside the pressure sensors. Conducting flow and pressure mea-
 673 surements below this pressure, or even at negative pressures in the MPa range,
 674 as expected in plants, would require removal of all gas bubbles and any cavi-
 675 tation nuclei in the system, which has so far only been achieved in microscopic
 676 systems (Wheeler and Stroock, 2008; Pagay et al., 2014). Nevertheless, even at
 677 the modest range of sub-atmospheric pressures attainable in the current setup,
 678 we have been able to observe transient changes in twig water storage lasting for
 679 up to an hour, suggesting that this setup could be used to not only measure the
 680 hydraulic conductivity of plant segments very accurately, but also gain a better
 681 understanding of the role of water storage in the plant hydraulic system.

682 6 Conclusions

683 Current methods of measuring hydraulic conductivity of plant segments are
684 based on controlling a pressure gradient and pushing water through samples,
685 which does not reflect natural water transport processes in plants, i.e. suction-
686 driven flow with a pressure gradient determined by the flow rate imposed by leaf
687 water demand. Here we describe two new experimental approaches to measure
688 hydraulic conductivity using suction and a controlled flow rate. The artificial
689 plant setup, consisting of an artificial root, an artificial leaf and a plant segment
690 in the flow path between the two, is well suited for educational purposes, as its
691 components are intuitively comparable to real plant organs. The syringe pump
692 setup, where the evaporating artificial leaf is replaced by a syringe pump, is more
693 versatile for conducting scientific experiments. Our detailed tests of the setup
694 confirmed that the conductivity values obtained are similar to those measured
695 with the traditional Sperry method when similar flow rates are used. However,
696 due to the use of a flow meter before the twig and syringe pump controlled
697 suction at the other end, the setup enables quantifying changes in twig water
698 storage. We found that simulating water stress by increasing flow resistance
699 at the source or flow rate at the sink both resulted in transient withdrawal of
700 water from the twig, which was largely reversible, i.e. the twig replenished its
701 storage to the original value when original flow conditions were restored. This
702 enables unique insights into the interplay between pressure, flow rate, hydraulic
703 conductivity and water storage in plant segments.

704 7 Data availability

705 All data and analysis code is available at <https://doi.org/10.5281/zenodo.7322605>.

References

- Alder, N. N., Pockman, W. T., Sperry, J. S., and Nuismer, S. (1997). Use of centrifugal force in the study of xylem cavitation. *Journal of Experimental Botany*, 48(3):665–674.
- Bär, A., Nardini, A., and Mayr, S. (2018). Post-fire effects in xylem hydraulics of *Picea abies*, *Pinus sylvestris* and *Fagus sylvatica*. *New Phytologist*, 217(4):1484–1493. Publisher: John Wiley & Sons, Ltd.
- Bonetti, S., Breitenstein, D., Fatichi, S., Domec, J.-C., and Or, D. (2021). Persistent decay of fresh xylem hydraulic conductivity varies with pressure gradient and marks plant responses to injury. *Plant, Cell & Environment*, 44(2):371–386.
- Buchmüller, K. S. (1986). Jahrringcharakteristik und Gefäßslängen in *Fagus sylvatica* L.I. *Vierteljahrsschrift der Naturforschenden Gesellschaft in Zürich*, 131(3):161–182.
- Canny, M. J. (1998). Transporting water in plants. *American Scientist*, 86:152–159.
- Canny, M. J., Sparks, J. P., Huang, C. X., and Roderick, M. L. (2007). Hypothesis: Air embolisms exsolving in the transpiration water—the effect of constrictions in the xylem pipes. *Functional plant biology*, 34(2):95–111.
- Caquet, B., Barigah, T. S., Cochard, H., Montpied, P., Collet, C., Dreyer, E., and Epron, D. (2009). Hydraulic properties of naturally regenerated beech saplings respond to canopy opening. *Tree Physiology*, 29(11):1395–1405. Publisher: Oxford Academic.
- Choat, B., Jansen, S., Brodribb, T. J., Cochard, H., Delzon, S., Bhaskar, R., Bucci, S. J., Feild, T. S., Gleason, S. M., Hacke, U. G., Jacobsen, A. L., Lens, F., Maherali, H., Martínez-Vilalta, J., Mayr, S., Mencuccini, M., Mitchell, P. J., Nardini, A., Pittermann, J., Pratt, R. B., Sperry, J. S., Westoby, M., Wright, I. J., and Zanne, A. E. (2012). Global convergence in the vulnerability of forests to drought. *Nature*, 491(7426):752–755. Number: 7426 Publisher: Nature Publishing Group.
- Cochard, H. (2002). A technique for measuring xylem hydraulic conductance under high negative pressures. *Plant, Cell & Environment*, 25(6):815–

819. _eprint: <https://onlinelibrary.wiley.com/doi/pdf/10.1046/j.1365-3040.2002.00863.x>.
- Cochard, H., Badel, E., Herbette, S., Delzon, S., Choat, B., and Jansen, S. (2013). Methods for measuring plant vulnerability to cavitation: a critical review. *Journal of Experimental Botany*, 64(15):4779–4791.
- Dixon, H. H. and Joly, J. (1895). On the ascent of sap.
- Hölttä, T., Cochard, H., Nikinmaa, E., and Mencuccini, M. (2009). Capacitive effect of cavitation in xylem conduits: results from a dynamic model. *Plant, Cell & Environment*, 32(1):10–21.
- Kolb, K., Sperry, J., and Lamont, B. (1996). A method for measuring xylem hydraulic conductance and embolism in entire root and shoot systems. *Journal of Experimental Botany*, 47(304):1805–1810. Publisher: Oxford University Press.
- McDowell, N. G., Brodribb, T. J., and Nardini, A. (2019). Hydraulics in the 21st century. *New Phytologist*, 224(2):537–542.
- Nardini, A., Salleo, S., and Jansen, S. (2011). More than just a vulnerable pipeline: xylem physiology in the light of ion-mediated regulation of plant water transport. *Journal of Experimental Botany*, 62(14):4701–4718.
- Pagay, V., Santiago, M., Sessoms, D. A., Huber, E. J., Vincent, O., Pharkya, A., Corso, T. N., Lakso, A. N., and Stroock, A. D. (2014). A microtensiometer capable of measuring water potentials below -10 MPa. *Lab on a Chip*, 14(15):2806–2817. Publisher: The Royal Society of Chemistry.
- Pratt, R. B., Castro, V., Fickle, J. C., Madsen, A., and Jacobsen, A. L. (2020). Factors controlling drought resistance in grapevine (*Vitis vinifera*, chardonnay): application of a new microCT method to assess functional embolism resistance. *American Journal of Botany*, 107(4):618–627. _eprint: <https://bsapubs.onlinelibrary.wiley.com/doi/pdf/10.1002/ajb2.1450>.
- Rosner, S., Heinze, B., Savi, T., and Dalla-Salda, G. (2019). Prediction of hydraulic conductivity loss from relative water loss: new insights into water storage of tree stems and branches. *Physiologia Plantarum*, 165(4):843–854. Publisher: John Wiley & Sons, Ltd.

769 Shi, W., Dalrymple, R. M., McKenny, C. J., Morrow, D. S., Rashed, Z. T.,
770 Surinach, D. A., and Boreyko, J. B. (2020). Passive water ascent in a tall,
771 scalable synthetic tree. *Scientific Reports*, 10(1).

772 Sperry, J. S. (1986). Relationship of Xylem Embolism to Xylem Pressure Po-
773 tential, Stomatal Closure, and Shoot Morphology in the Palm *Rhapis excelsa*
774 1. *Plant Physiology*, 80(1):110–116.

775 Sperry, J. S., Donnelly, J. R., and Tyree, M. T. (1988). A method for measuring
776 hydraulic conductivity and embolism in xylem. *Plant, Cell & Environment*,
777 11(1):35–40.

778 Torres-Ruiz, J. M., Sperry, J. S., and Fernández, J. E. (2012). Improving
779 xylem hydraulic conductivity measurements by correcting the error caused
780 by passive water uptake. *Physiologia Plantarum*, 146(2):129–135. eprint:
781 <https://onlinelibrary.wiley.com/doi/pdf/10.1111/j.1399-3054.2012.01619.x>.

782 Tsuda, M. and Tyree, M. T. (2000). Plant hydraulic conductance measured by
783 the high pressure flow meter in crop plants. *Journal of Experimental Botany*,
784 51(345):823–828.

785 Tyree, M. T., Patiño, S., Bennink, J., and Alexander, J. (1995). Dynamic
786 measurements of roots hydraulic conductance using a high-pressure flowmeter
787 in the laboratory and field. *Journal of Experimental Botany*, 46(1):83–94.

788 Tyree, M. T., Sinclair, B., Lu, P., and Granier, A. (1993). Whole shoot hydraulic
789 resistance in *Quercus* species measured with a new high-pressure flowmeter.
790 *Annales des Sciences Forestières*, 50(5):417–423. Publisher: EDP Sciences.

791 Tyree, M. T. and Sperry, J. S. (1988). Do Woody Plants Operate Near the
792 Point of Catastrophic Xylem Dysfunction Caused by Dynamic Water Stress?:
793 Answers from a Model. *Plant Physiology*, 88(3):574–580.

794 Tyree, M. T. and Yang, S. (1992). Hydraulic Conductivity Recovery versus
795 Water Pressure in Xylem of *Acer saccharum*. *Plant Physiology*, 100(2):669–
796 676. Publisher: American Society of Plant Biologists (ASPB).

797 Tyree, M. T. and Zimmermann, M. H. (2002). The Cohesion-Tension Theory
798 of Sap Ascent. In Tyree, M. T. and Zimmermann, M. H., editors, *Xylem*
799 *Structure and the Ascent of Sap*, Springer Series in Wood Science, pages 49–
800 88. Springer, Berlin, Heidelberg.

- 801 Venturas, M. D., Sperry, J. S., and Hacke, U. G. (2017). Plant xylem
802 hydraulics: What we understand, current research, and future chal-
803 lenges. *Journal of Integrative Plant Biology*, 59(6):356–389. _eprint:
804 <https://onlinelibrary.wiley.com/doi/pdf/10.1111/jipb.12534>.
- 805 Wheeler, J. K., Huggett, B. A., Tofte, A. N., Rockwell, F. E., and
806 Holbrook, N. M. (2013). Cutting xylem under tension or supersatu-
807 rated with gas can generate PLC and the appearance of rapid recovery
808 from embolism. *Plant, Cell & Environment*, 36(11):1938–1949. _eprint:
809 <https://www.onlinelibrary.wiley.com/doi/pdf/10.1111/pce.12139>.
- 810 Wheeler, T. D. and Stroock, A. D. (2008). The transpiration of water at negative
811 pressures in a synthetic tree. *Nature*, 455(7210):208–212.
- 812 Zimmermann, U., Haase, A., Langbein, D., and Meinzer, F. (1993). Mecha-
813 nisms of Long-Distance Water Transport in Plants: A Re-Examination of
814 Some Paradigms in the Light of New Evidence. *Philosophical Transactions:*
815 *Biological Sciences*, 341(1295):19–31.
- 816 Zweifel, R., Item, H., and Häsler, R. (2001). Link between diurnal stem radius
817 changes and tree water relations. *Tree Physiology*, 21(12-13):869–877.